CARBON 78 (2014) 181–189

Available at www.sciencedirect.com

ScienceDirect

journal homepage: www.elsevier.com/locate/carbon

Structure and stability of graphene edges in O_2 and H_2 environments from ab initio thermodynamics

G.J. Soldano [a,*], M.F. Juarez [b], B.W.T. Teo [c], E. Santos [b,d]

[a] Departamento de Matemática y Física – UNC, Córdoba, Argentina
[b] Institute of Theoretical Chemistry, Ulm University, D-89069 Ulm, Germany
[c] Department of Chemistry, National University of Singapore, Singapore
[d] Facultad de Matemática Astronomía y Física, Instituto de Física Enrique Gaviola (IFEGCONICET), Universidad Nacional de Córdoba, 5000 Córdoba, Argentina

ARTICLE INFO

Article history:
Received 12 December 2013
Accepted 28 June 2014
Available online 7 July 2014

ABSTRACT

Edges play a determining role in the electronic and transport properties of graphene, however, their actual morphology and configuration remain unknown. Using ab initio thermodynamics, we have systematically studied the stability and structure of armchair and zigzag edges of graphene in pure O_2 and combined O_2 and H_2 environments. In total, 81 different nanostructures were investigated, however, only a few of them domain the phase diagram. Our calculations show that zigzag edges are less stable than armchair edges. Nonetheless, the former exhibit a much richer diversity in terms of structures. The oxygen-terminated edges occupy the largest regions in the phase stability diagram in comparison with hydrogen-oxygen-terminated edges, which correspond to carboxyl and alcohol functional groups.

1. Introduction

Graphene nanoribbons (GNRs) are bidimensional strips of isolated graphite layers (graphene) featuring widths at the nanometer scale. The structural boundary conditions imposed by their width provide them with unique electrical [13,29,14,6], optical [22], thermal [3], and mechanical [24] properties. Moreover, these properties can be tuned by the width of the strips. Recent theoretical and experimental works show that the band gap of these semiconducting nanoribbons decrease with their width [14,6]. It is clear then that GNRs offer a great utility for future electronic devices. In fact, GNRs could increase by more than 10,000 times the number of transistors per area in computer chips. However, before the fabrication process can be scaled up, it is essential to provide control in the synthesis of GNRs, a task that remains unsolved. Most of the approaches to produce GNRs are top-down techniques, which implies only limited control over their size and structure [16,8,38,30,27,43,10,9,21,18,17,5]. Nonetheless, a great improvement has been made with bottom-up synthesis using molecular precursors. With this method it was possible to synthesize 7-atoms-wide [4] and 13-atoms-wide [7] GNRs. The edges of graphene are more reactive than the pristine basal plane [42,44]. Indeed, GNRs are an excellent platform for functionalization [1,45,26]. While it is known from experimental studies, which functional groups can be found at the

* Corresponding author.
E-mail address: gersoldano@gmail.com (G.J. Soldano).
http://dx.doi.org/10.1016/j.carbon.2014.06.070
0008-6223/

edges of GNRs (carboxyls, anhydrates, lactones, phenols, lactols, pyrones and ketones [37,12,11,23,2]), their actual arrangement and abundance still remains unknown. This is an ideal scenario for ab initio thermodynamics [32] since, relying on state-of-the-art quantum-chemistry calculations, one can estimate which structures shall predominate at a given chemical potential (or pressure). To stress the importance of theoretical studies, it is instructive to remember that the unusual electronic and magnetic properties of GNRs were first theoretically predicted [13,29] and only then experimentally verified.

Here, we present a theoretical approach to the structure and stability of graphene edges in an environment containing H_2 and/or O_2. Several studies can be related to this work. Lee investigated the interaction between vicinal functional groups [25]. It was found that for OH terminations the interaction is attractive, while for NH_2, COOH, CN, C_6H_6 it is repulsive. The thermodynamics and kinetics of O_2 chemisorption have been studied on graphene clusters and carbon nanotubes [36]. It was concluded that oxygen dissociates on armchair edges, while on zigzag the adsorption is non-dissociative.

Seitsonen et al. investigated the structure and stability of such edges in O_2, CO_2, H_2O, and NH_3 environments by ab initio thermodynamics [35]. Due to the large number of possible structures they restricted their work to O/H/N contents as fixed by the respective molecular stoichiometries. However, there is no such restriction in nature. Still, several structures where evaluated and only few resulted stable: armchair lactone in the case of oxygen, and a zigzag edge in the case of water and ammonia.

Another approach was made by Vanin et al. [41], who studied the stability of five different edge geometries in the presence of common gases. They showed that the saturation of zigzag, and armchair by atomic oxygen and hydrogen are the most stable for GNRs. Since the topic was to compare the stability of different edges, only one structure was evaluated for each edge containing oxygen, hydrogen, nitrogen, and other passivating elements.

Besides the comparatively smaller amount of structures tested, a common limitation in the latter works is that entropy was not considered in the calculation of the free energy. To the best of our knowledge, in the present work ab initio thermodynamics of GNRs is performed for the first time without imposing any restriction on the O/H content and including the vibrational entropy into the edge free energy.

This work is organized as follows: in Section 2, we provide the details of the modeling and the set-up of the density functional theory (DFT) calculations, the procedure to obtain the edge free energy, and the strategy to discard unstable structures without any computational cost. In Section 3, the most stable edge structures found in this work are shown for two different environments: oxygen and hydrogen–oxygen atmospheres. Finally, the conclusions are given in Section 4. In addition, all the details regarding energetic convergence criteria, vibrational considerations, and some unstable structures which are not shown here are provided in the Supporting information.

2. Theory

2.1. Modeling and first-principles calculations

We modeled the GNRs as graphene sheets which are periodic in one dimension (*x* axis) and truncated by two edges (*y* axis). The edges correspond to the so-called armchair and zigzag configurations. One side of the nanoribbon is bonded to the species of interest while the other side is closed with hydrogen atoms. The gap distance between the periodic edges and between graphene planes is 12 Å. The width of the nanoribbon (from edge to edge) was optimized by increasing the number of carbon atoms along the y axis until the change in the edge free energy (explained below) for a two-side hydrogen-terminated graphene was less than 0.01 eV Å^{-1}. For this purpose, a distance of 9.27 Å for zigzag edges and of 8.03 Å for armchair edges suffices (see Supporting information). The carbon–carbon distance was taken from the optimized graphene lattice constant of 2.46 Å, which is in excellent agreement with experimental values [19].

All calculations were performed using DACAPO [15], a DFT code. The electron-ion interactions were accounted through ultrasoft pseudopotentials [40], while the valence electrons were treated within the generalized gradient approximation (GGA) in the version of Perdew, Burke and Ernzerhof (PBE) [31]. An energy cutoff of 450 eV was used with a $(12 \times 1 \times 1)$ k-points Monkhorst–Pack grid [28] for zigzag and armchair unit cells. In any case, an increase by 1 k-point, or by 50 eV in the energy cutoff, led to a negligible change in energy of 5 meV. For the relaxations the convergence criterion was achieved when the total forces were less than 10 meV Å^{-1}. All the atoms were fully relaxed. Little change was observed for the hydrogenated edge, and no graphene-sheet corrugation was found.

Regarding the vibrational contributions to the free energy, we have determined the vibrational frequencies for the edge atoms of the nanoribbons by nonequivalent displacements in different directions freezing the remaining atoms in the equilibrium configuration. The harmonic frequencies at the gamma point were calculated by diagonalizing the mass-weighted Hessian matrix, obtained by numerical differentiation of the analytical gradient with respect to the atomic coordinates. Only the displacements of the edge atoms of the nanoribbons were considered while freezing the remaining atoms in their corresponding equilibrium configuration. We have found that a very accurate approximation is achieved if only the adatoms and their closer carbon atoms up to second neighbors are allowed to vibrate (see Supporting information).

2.2. Edge free energy, and search strategy

We have determined the stability of several GNRs at a finite temperature and pressure in the framework of first-principles atomistic thermodynamics [32]. The environment acts as a reservoir, therefore, taking/adding atoms from/to the edge does not change the temperature or the pressure. In ab initio thermodynamics, it is common to use the term *surface free energy* since the topic of study is the surface of a structure.

In the latter case the free energy is normalized by the area of the surface. In this work however, we are interested in the configurations of the *edge* of graphene; therefore, it is more suited to use the term *edge free energy* (γ). In contrast with the former case, the free energy is normalized by the length of the edge (L). The expression for γ is the following

$$\gamma(T,p) = \frac{1}{L}\left[G_{GNR} - n_C G_{gph} - n_H \mu_H - n_O \mu_O\right] - \gamma_H \quad (1)$$

where G_{GNR} is the Gibbs free energy of a graphene nanoribbon with n_C, n_H, and n_O carbon, hydrogen, and oxygen atoms, respectively; G_{gph} is the Gibbs free energy per atom of the infinite graphene layer, μ_H and μ_O are the chemical potentials of hydrogen and oxygen, respectively. Since we are only interested in the oxidized side of the nanoribbon, the energy of forming the hydrogen-terminated side (γ_H) must be subtracted. This is calculated by

$$\gamma_H(T,p) = \frac{1}{2L}\left[G_H - n_C G_{gph} - n_H \mu_H\right] \quad (2)$$

where G_H is the Gibbs free energy of the graphene nanoribbon fully closed by hydrogen. The factor of two accounts for the two edges.

The Gibbs and the Helmholtz free energies (F) are related by

$$G = F + pV \quad (3)$$

However, the pV term is negligible as long as the pressure is below 100 atm (where it keeps in the order of 0.1 meV). In turn, the Helmholtz free energy is defined as

$$F = E^{DFT} + F^{vib} \quad (4)$$

where E^{DFT} is the total energy (electronic + ionic) obtained by DFT and it can be interpreted as the Helmholtz free energy of the system at zero temperature and neglecting zero-point vibrations. F^{vib} is the vibrational contribution to the Helmholtz free energy, it depends on the vibrational modes ω_i and the temperature T via

$$F^{vib} = -\frac{\hbar}{2}\sum_i \omega_i + k_B T \sum_i \ln\left[\exp\left(\frac{\hbar\omega_i}{k_B T}\right)\right] \quad (5)$$

where $\hbar$ and k_B are the reduced Planck and Boltzmann constants, respectively. The first term corresponds to the zero-point energy and the second to the entropy. In summary, the expression for the Gibbs free energy can be reduced to

$$G(\omega_i, T) = E^{DFT} + F^{vib}(\omega_i, T) \quad (6)$$

In addition to the total energy, the vibrational frequencies have to be evaluated, which can be also done using DFT calculations.

The chemical potential of oxygen is obtained by

$$\mu_O = \frac{1}{2}\left[E^{DFT}_{O_2} + E^{ZPE}_{O_2} + \mu^0_{O_2}(T,p^0) + k_B T \ln\left(\frac{p_{O_2}}{p^0}\right)\right] \quad (7)$$

where $E^{ZPE}_{O_2}$ is the zero-point energy of the oxygen molecule. Correspondingly, the chemical potential of hydrogen is given by

$$\mu_H = \frac{1}{2}\left[E^{DFT}_{H_2} + E^{ZPE}_{H_2} + \mu^0_{H_2}(T,p^0) + k_B T \ln\left(\frac{p_{H_2}}{p^0}\right)\right] \quad (8)$$

For convenience, we can rewrite Eq. (1) as

$$\gamma(T,p) = \frac{1}{L}\left[G_{GNR}(T) - n_C G_{gph}(T)\right] - \rho_H \mu_H(p) - \rho_O \mu_O(p) - \gamma_H(p) \quad (9)$$

where $\rho_x = n_x/L$ is the hydrogen or oxygen density. The density of x (x = H, O) determines the slope of γ vs. μ_x.

A useful expression that we shall use is the formation energy

$$E_f = \frac{1}{L}\left[E_{GNR} - n_C E_{gph} - n_H E_{H_2}/2 - n_O E_{O_2}/2\right] - E_{f_H} \quad (10)$$

where E_{f_H} is the formation energy of the other border of graphene, terminated with hydrogen atoms:

$$E_{f_H} = \frac{1}{2L}\left[E_{HGNR} - n_C E_{gph} - n_H E_{H_2}/2\right] \quad (11)$$

These energies correspond to total DFT energies, neglecting the contributions of vibrations, temperature, and pressure. According to its definition, the lower the formation energy the higher the stability of the structure. A negative value of the edge free energy corresponds to an exergonic process. We can rewrite Eq. (9) as

$$\gamma(T,p) = E_f + \Delta F^{vib}(T) - \rho_H(\mu_H(p) - E_{H_2}/2) - \rho_O(\mu_O(p) - E_{O_2}/2) - (\gamma_H(p) - E_{f_H}) \quad (12)$$

where the entropic term ΔF^{vib} has been defined as

$$\Delta F^{vib}(T) = \frac{1}{L}\left[F^{vib}_{GNR}(T) - n_C F^{vib}_{gph}(T)\right] \quad (13)$$

In this manner, we have decomposed the edge free energy γ in their main parts: the total energy (electronic + ionic) E_f, the entropic energy ΔF^{vib} (mainly due to the vibrational frequencies in the nanoribbon), and the terms on account of oxygen and hydrogen chemical potentials. Now, let us determine an expression for the formation energy difference ΔE_f and the edge free energy difference $\Delta\gamma$ for two species (A and B) with the same hydrogen and oxygen density. Since ρ_H and ρ_O are the same then

$$\Delta E_f = E_{f,A} - E_{f,B} = \frac{1}{L}\left[\Delta E_{GNR} - \Delta n_C E_{gph}\right] \quad (14)$$

$$\Delta\gamma(T) = \frac{1}{L}\left[\Delta G_{GNR}(T) - \Delta n_C G_{gph}(T)\right] \quad (15)$$

using Eq. (6) in $\Delta\gamma$ and regrouping gives

$$\Delta\gamma(T) = \frac{1}{L}\left[\Delta E_{GNR} - \Delta n_C E_{gph} + (F^{vib}_A(T) - F^{vib}_B(T))\right] \quad (16)$$

where F^{vib} contains the vibrational terms of each system. Since the latter difference is considerably smaller than the other terms, it can be neglected, which gives nothing but the formation energy difference

$$\Delta\gamma \approx \Delta E_f \quad (17)$$

Thus, by comparing the formation energy of two edges with the same H and O density, one can estimate the difference in their edge free energy.

At this point, it is important to explain the strategy to find stable graphene nanoribbons. It is extremely demanding, if not virtually impossible, to cover all the possible hydrogen-oxygen combinations of graphene edges [35]; however, we can anticipate whether the edge free energy of a certain structure is worth performing or not. As it is deduced from Eq. (17), if structure A and B have the same oxygen density, and $E_f(A) \ll E_f(B)$, then A is more stable than B in the whole interval of μ_O. Therefore, it is not necessary to calculate the edge free energy of structure B. We restricted our study to systems with a maximum of three unit cells along the edge. We have

not concerned ourselves with the reaction processes to produce such structures, since the kinetics are not within the scope of this work.

Finally, a brief remark is made concerning the thermodynamic limits for hydrogen and oxygen chemical potentials. The upper limits are given by the chemical potential at which both hydrogen and oxygen molecules are formed, which is our reference potential for both species ($\mu_H = \mu_O = 0$). We have chosen as the lower limits those hydrogen and oxygen chemical potentials that are accessible experimentally at very high temperatures (900 K).

3. Results

The schemes of the most stable nanoribbon edges found in this work are shown in Fig. 1. The structures are sorted by increasing oxygen and hydrogen densities (ρ_O and ρ_H, respectively) and increasing formation energy. First, the bare edges, hydrogen-terminated and oxygen-terminated edges are presented. Following on, several possible combinations of hydrogen- and oxygen-terminated edges are illustrated.

Let us start with the bare edges. The zigzag unreconstructed edge (z_0) was found to be spin-polarized due to dangling bonds. The unpolarized zigzag edge is 0.18 eV Å^{-1} higher in energy with respect to the polarized zigzag edge. In contrast, the reconstructed zigzag edge (z_{57}), proposed by Koskinen et al. [20] is not magnetic. This structure forms triple bonds and wider bond angles, making it the most stable pure carbon edge of graphene. The armchair edge (a_0) also does not present magnetic properties since in this case the uncoordinated carbon atoms are first-neighbors, and can therefore make a triple bond between them. Calculations of spin were also performed for several structures but, unless mentioned, none of the other edges presented here possess magnetic properties.

Regarding the formation energy, it was found that for those conformations with strong carbon–oxygen bonds, such us ketones, carboxyls, and alcohols, a clear linear trend is observed with respect to the oxygen density. Structures with higher oxygen density have lower formation energies (see Supporting information).

In our study, we have also considered the molecular adsorption of H_2O and O_2. However, none of them resulted

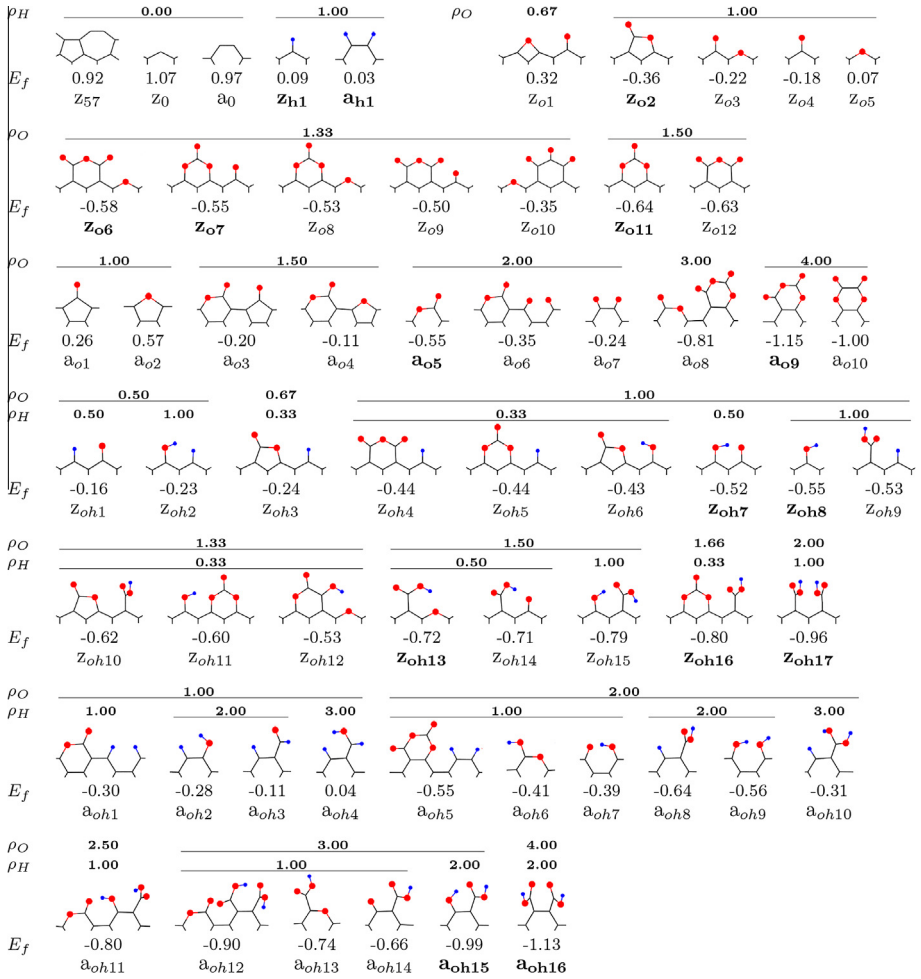

Fig. 1 – Schematic configuration, labeling oxygen/hydrogen density (ρ_O/ρ_H) by number of oxygen/hydrogen atoms per unit cell, and formation energy (E_f) in eV Å^{-1} for oxygen- and hydrogen-terminated edges of armchair and zigzag graphene nanoribbons. The structures shown above are periodic throughout the nanoribbon edges. Hydrogen and oxygen atoms are represented using blue and red circles, respectively, while the graphene edge is represented by lines connecting first neighbors. The label of relevant structures are highlighted in bold text. (A colour version of this figure can be viewed online.)

in stable configurations in comparison with other structures having equal oxygen and/or hydrogen density. In fact, all the investigated molecular adsorptions show positive E_f (endothermic). More information about these and other unstable configurations are provided in the Supporting information.

3.1. Oxygen-containing environment

As we can see from the oxygen-terminated edges in Fig. 1, several nanoribbons show negative free energies, the lowest correspond to z_{o11} for zigzag and a_{o9} for armchair edges.

The thermodynamic stability diagram for graphene nanoribbons in a pure O_2 atmosphere at 300 K is shown in Fig. 2. Only the most stable armchair, zigzag, and bare edges are presented. Note that for bare edges ρ_O is equal to zero, so that they appear as horizontal lines in the diagram.

For armchair GNRs, the stable edges are: a_{o5}, a_{o8}, and a_{o9}. However, only two have the lowest energies, dominating the phase diagram: a_{o9} at high oxygen pressure and a_{o5} at lower pressure. Meanwhile, for zigzag edges, three stable structures emerge: z_{o2} at low oxygen chemical potential, z_{o6} at intermediate potentials, and z_{o11}/z_{o12} at higher chemical potential. The formation energy of z_{o12} is only 0.01 eV Å^{-1} higher than that of z_{o11}, and even with entropic considerations it is hard to predict which one is more stable. None of these zigzag nanoribbons are more stable than a_{o5} or a_{o9} within the oxygen chemical potential limits. This indicates that only two armchair edges should be stable in an oxygen environment from ultra-high vacuum to high pressures.

At lower μ_O, z_{o2} is more stable than z_{o6} although the formation energy of z_{o2} is 0.22 eV Å^{-1} higher than that of z_{o6} (see Fig. 1). This is due to the fact that z_{o2} has a relative lower oxygen density and consequently shows a lower slope in Fig. 2.

We have also found that neglecting the vibrational entropy leads to some changes in the thermodynamic stability diagram, the most important of which is the appearance of z_{o2} as the most stable edge at low oxygen potentials (see Supporting information).

Some oxygen-terminated structures in Fig. 1 have been already studied by Seitsonen et al. [35] (labeled differently) although without taken into account of the entropy effect. The calculated formation energies in our study are in good agreement with their reported work. However, small differences in edge free energies were found which we attribute to the vibrational entropy. To the best of our knowledge, none of the edge free energy curves presented in Fig. 2 have been reported before, with the exception of a_{o5} and the bare edges [35].

3.2. Hydrogen–oxygen-containing environment

In this section we extend our analysis to the two-component environment, H_2 and O_2. Since now the edge free energy γ depends on both μ_H and μ_O, the two-dimensional graph in Fig. 2 turns into a three-dimensional one. If we project the lowest edge free energies of such a graph onto the $\mu_H\mu_O$-plane, the stability regions of the most stable phases are obtained, which are shown in Fig. 3. The zigzag and the armchair edge-terminations are shown separately and for three different temperatures: 100 K, 300 K, and 600 K.

In this case an additional constraint for the thermodynamic limits appears since the combination of H_2 and O_2 can produce water [39], therefore

$$\mu_O + 2\mu_H < \Delta H_f(H_2O) \tag{18}$$

where the formation energy of water is $\Delta H_f(H_2O) = -2.34$ eV. Eq. (18) defines the line shown in Fig. 3, whereby water condensates. Nevertheless, the gas phase reaction $H_2 + 1/2O_2 \rightarrow H_2O$ is kinetically hindered, allowing us to neglect it in our study. Thus, we shall consider a "constrained thermodynamic equilibrium" [33] in which H_2 and O_2 are in thermodynamic equilibrium with graphene nanoribbons individually, while H_2 and O_2 in the gas phase are not. We will refer to

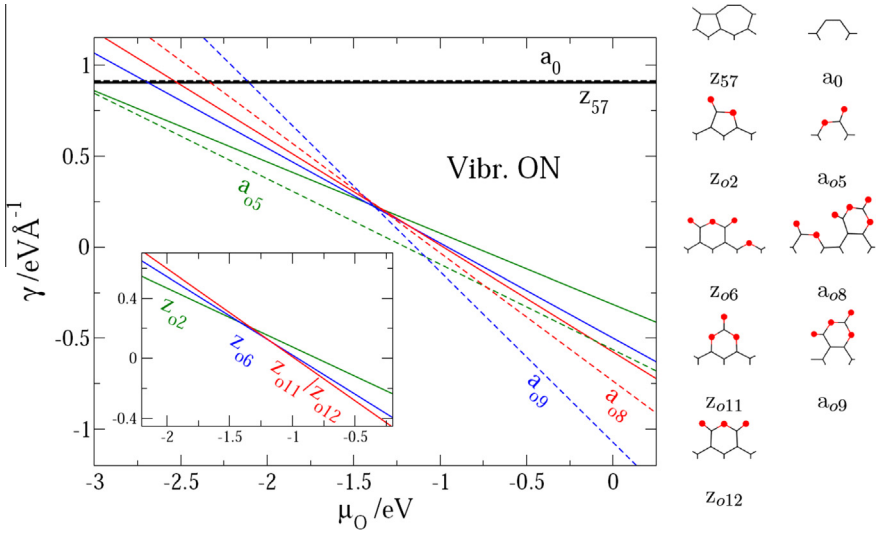

Fig. 2 – Edge free energy of the most stable oxygen-terminated graphene nanoribbons versus the oxygen chemical potential at 300 K. For clarity, results for zigzag edges are shown in the inset. The corresponding structures are also illustrated at the right. (A colour version of this figure can be viewed online.)

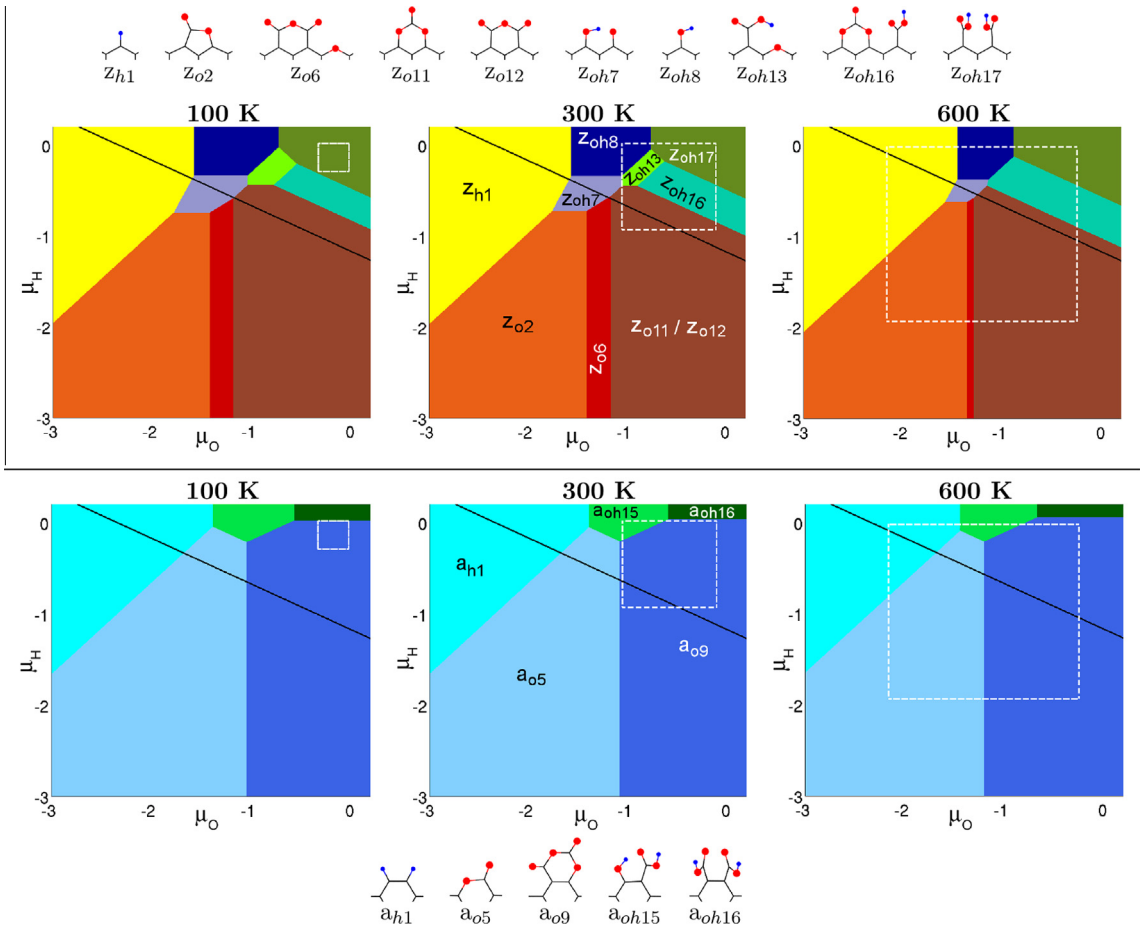

Fig. 3 – Surface phase diagram of stable hydrogen- and oxygen-terminated graphene nanoribbons as a function of chemical potentials (in eV) for three temperatures. Top and bottom phase diagrams correspond to zigzag and the armchair edges, respectively. The oblique line marks the stability limit of structures with respect to water formation; species above this line are metastable. Inside the dashed square are the pressures accessible experimentally (10^{-13} to 10^{3} atm). The corresponding structures are also shown above and below the diagrams. (A colour version of this figure can be viewed online.)

the upper part of the condensation line as the metastable region, and the lower one as the stable region.

For armchair and zigzag configurations, oxygen-terminated edges occupy a larger region in the diagram as compared to the hydrogen–oxygen edges. This is because oxygen–carbon bond is more stable than both the hydrogen–carbon bond and the hydroxyl-carbon bond.

The armchair edges exhibit a rather poor diversity of compounds in terms of structure in comparison with zigzag edges as shown in the surface phase diagram. The entire stable region is only dominated by three structures: a_{h1}, a_{o5}, and a_{o9}. Only two combined hydrogen–oxygen edges appear in the metastable region (a_{oh15} and a_{oh16}), and both of them contain carboxyl functional groups. Changes in temperature from 100 to 600 K have a negligible effect on the armchair edges, while on zigzag ribbons some differences are observed.

On the other hand, for zigzag edges several phases were found to be stable in the phase diagram. The stable region is predominantly occupied by three oxygen-terminated edges (z_{o2}, z_{o6}, and z_{o11}/z_{o12}); one hydrogen-terminated edge (z_{h1}); and one combined hydrogen–oxygen-terminated edge (z_{oh07}), which consists of the alternation of an alcohol and a ketone. The latter is the only combined edge found below the condensation line in the phase diagram. Several stable phases were also found in the metastable region, all of them contain carboxyl or/and hydroxyl functional groups.

We have found that armchair ribbons are more stable than the zigzag ones, so that if both edges were compared in the same surface phase diagram, only the armchair structures would emerge (bottom of Fig. 3).

The dashed squares in Fig. 3 mark the experimental limit, which is the limit of achieving the O_2 and H_2 pressure experimentally. If zigzag and armchair edges could be obtained separately, only one zigzag (z_{oh17}) and one armchair edge (a_{o9}) would be observable at 100 K. However, at higher temperatures, the size of the dashed square box increases, and thus almost every conformation of armchair and zigzag edges shown in the phase diagrams would be observable experimentally.

In order to explain the trends observed in the phase diagrams of Fig. 3, we have decomposed the edge free energy γ in Table 1. According to Eq. (12), we have explicitly calculated

Table 1 – Formation energies E_f and energy differences of the vibrational contribution to the Helmholtz free energy. The selected systems correspond to the stable structures at temperature $T = 300$ K and experimentally accessible pressures, according to Fig. 3. All the energies are in eV Å^{-1}.

	ρ_H	ρ_O	E_f	ΔF^{vib} (100 K)	ΔF^{vib} (300 K)	ΔF^{vib} (600 K)
Arm						
a_{oh16}	2.0	4.0	−1.132	0.149	0.136	0.068
a_{oh15}	2.0	3.0	−0.995	0.143	0.135	0.085
a_{o9}	0.0	4.0	−1.152	0.077	0.057	−0.021
zz						
z_{oh17}	1.0	2.0	−0.958	0.198	0.185	0.118
z_{oh16}	0.33	1.66	−0.802	0.103	0.093	0.046
z_{oh13}	0.5	1.5	−0.722	0.060	0.057	0.033
z_{oh08}	1.0	1.0	−0.553	0.061	0.059	0.042
z_{o12}	0.0	1.5	−0.634	0.038	−0.001	−0.06
z_{o11}	0.0	1.5	−0.635	0.053	0.052	0.035

the terms corresponding to the total energy (E_f) and to the entropic contributions (ΔF^{vib}), defined in Eqs. (10) and (13), respectively. The terms corresponding to the chemical potentials in Eq. (9) have not been included in the table because they are constant (at a given pressure p, and temperature T). Instead, the oxygen and hydrogen densities ρ_O and ρ_H are displayed.

The entropic contribution is significantly important in structures with lighter atoms (like hydrogen) or less coordinated groups (like alcohols or ketones) because of their larger vibrational frequencies (see a_{oh16}, z_{oh17}, and z_{oh16}). In particular, the temperature effect on the entropy can explain the disappearance of z_{oh13} from the phase diagram at 600 K. The values in Table 1 show that the structures z_{oh16} and z_{oh13} have similar formation energies as well as oxygen and hydrogen densities. Nevertheless, at higher temperatures, the entropy favors z_{oh16}, since the vibrational frequencies of z_{oh16} are larger than that of z_{oh13}. A similar behavior is observed for the edges z_{o11} and z_{o12}, which are almost isoenergetic at 300 K.

In general, structures with low formation and vibrational energies dominate the phase diagram. However, their final distribution depends on their oxygen and hydrogen densities. Carboxylic groups have the highest formation energies but their high oxygen and hydrogen contents make them stable only in the regions with high pressures (high chemical potentials). A clear example of this observation is the structure a_{o9}, that has a low formation energy and is stable in a wide region of the diagram, but becomes unstable at low μ_O. For the zigzag edges, some of the structures present in Table 1 have larger formation energies than the edges containing carboxylic groups (z_{oh17}, z_{oh16}). Nevertheless, the former systems dominate the phase diagrams due to their small ρ_O and ρ_H.

The ΔF^{vib} values are of the order of 0.2 eV Å^{-1} or less, which can be as much as the 20% of the E_f. It is therefore important to consider the entropic term in Eq. (4).

From Figs. 1 and 3 we can conclude that the calculated most stable combined hydrogen-oxygen-terminated edges for both zigzag and armchair structures are those fully terminated by carboxyl functional groups. In an experiment carried out by Salzmann et al. [34] carboxyl-terminated graphene nanoribbons were synthesized in a single oxidation procedure from single-wall carbon nanotubes and nitric acid. This experiment is in good agreement with our computational finding. We would expect these structures to occupy a larger region in the phase diagram of Fig. 3 in aqueous media, where the carboxyl groups can be further stabilized.

4. Conclusions

We have calculated surface phase diagrams from ab initio thermodynamics to predict the most stable graphene nanoribbon edges in oxygen and in hydrogen–oxygen environments. Overall, for both pure O_2 and combined O_2 and H_2 environments the armchair edges are more stable than the zigzag edges. Despite of the large number of possible edges studied (81), only few structures appear to be the most stable in a particular environment, all of them belong to armchair edges. The structures a_{o5} and a_{o9} are the most stable for an oxygen atmosphere. For a hydrogen–oxygen atmosphere these two edges occupied the largest portion of the phase diagram, followed by a_{h1}. Only two edges combining hydrogen and oxygen were found in the phase diagram: a_{oh15} and a_{oh16}, both containing carboxyl groups. In agreement with this finding, carboxyl-terminated nanoribbons have been observed experimentally.

In contrast, the chemistry of zigzag edges is far more diverse than that of the armchair edges. Four stable structures emerge as the most stable in an oxygen environment, and ten stable and metastable structures appear in the phase diagram for a hydrogen–oxygen environment. All the edges with hydrogen and oxygen combined appear in the metastable region, above which water can be formed, with the sole exception of z_{oh07}, a repeating unit of an alcohol and a neighboring ketone.

The vibrational contribution to the edge free energy plays an important role in both oxygen- and hydrogen–oxygen-terminated nanoribbons; therefore, it must be taken into account. Temperature has a negligible effect on the stable armchair edges, while on zigzag ribbons it may destabilize structures with relatively low vibrational frequencies.

We believe that all these findings bring some insights to experimentalists to gain a better understanding of the GNRs edges and therefore can aid in the controlling of the chemistry of such promising structures.

Acknowledgments

This work is part of the research network FOR1376 financed by the Deutsche Forschungsgemeinschaft. The content has been discussed in the internal meeting of this network. We thank PIP-CONICET 112-201001-00411 and PICT-2012-2324 (Agencia Nacional de Promoción Científica y Tecnológica, FONCYT, préstamo BID - Argentina) and a generous grant of computing time from the Baden-Württemberg grid is gratefully acknowledged.

Appendix A. Supplementary data

Supplementary data associated with this article can be found, in the online version, at http://dx.doi.org/10.1016/j.carbon.2014.06.070.

REFERENCES

[1] Acik Muge, Chabal Yves J. Nature of graphene edges: a review. Jpn J Appl Phys 2011;50:070101.
[2] Acik Muge, Lee Geunsik, Mattevi Cecilia, Pirkle Adam, Wallace Robert M, Chhowalla Manish, et al. The role of oxygen during thermal reduction of graphene oxide studied by infrared absorption spectroscopy. J Phys Chem C 2011;115:19761–81.
[3] Balandin Alexander A, Ghosh Suchismita, Bao Wenzhong, Calizo Irene, Teweldebrhan Desalegne, Miao Feng, et al. Superior thermal conductivity of single-layer graphene. Nano Lett 2008;8:902–7.
[4] Cai Jinming, Ruffieux Pascal, Jaafar Rached, Bieri Marco, Braun Thomas, Blankenburg Stephan, et al. Atomically precise bottom-up fabrication of graphene nanoribbons. Nature 2010;466:470–3.
[5] Campos Leonardo C, Manfrinato Vitor R, Sanchez-Yamagishi Javier D, Kong Jing, Jarillo-Herrero Pablo. Anisotropic etching and nanoribbon formation in single-layer graphene. Nano Lett 2009;9:2600–4.
[6] Chen Jian-Hao, Jang Chaun, Xiao Shudong, Ishigami Masa, Fuhrer Michael S. Intrinsic and extrinsic performance limits of graphene devices on SiO_2. Nat Nano 2008;3:206–9.
[7] Chen Yen-Chia, de Oteyza Dimas G, Pedramrazi Zahra, Chen Chen, Fischer Felix R, Crommie Michael F. Tuning the band gap of graphene nanoribbons synthesized from molecular precursors. ACS Nano 2013;7:6123–8.
[8] Chen Z, Lin Y-M, Rooks MJ, Avouris P. Graphene nano-ribbon electronics. Phys E: Low-Dimens Syst Nanostruct 2007;40:228–32.
[9] Ci Lijie, Xu Zhiping, Wang Lili, Gao Wei, Ding Feng, Kelly Kevin, et al. Controlled nanocutting of graphene. Nano Res 2008;1:116–22.
[10] Datta Sujit S, Strachan Douglas R, Khamis Samuel M, Charlie Johnson AT. Crystallographic etching of few-layer graphene. Nano Lett 2008;8:1912–5.
[11] Eda Goki, Chhowalla Manish. Chemically derived graphene oxide: towards large-area thin-film electronics and optoelectronics. Adv Mater 2010;22:2392–415.
[12] Fuente E, Menéndez JA, Díez MA, Suárez D, Montes-Morán MA. Infrared spectroscopy of carbon materials: a quantum chemical study of model compounds. J Phys Chem B 2003;107:6350–9.
[13] Fujita Mitsutaka, Wakabayashi Katsunori, Nakada Kyoko, Kusakabe Koichi. Peculiar localized state at zigzag graphite edge. J Phys Soc Jpn 1996;65:1920–3.
[14] Geim AK, Novoselov KS. The rise of graphene. Nat Mater 2007;6:183–91.
[15] Hammer B, Hansen LB, Nørskov JK. Improved adsorption energetics within density-functional theory using revised Perdew–Burke–Ernzerhof functionals. Phys Rev B 1999;59:7413–21.
[16] Han Melinda Y, Özyilmaz Barbaros, Zhang Yuanbo, Kim Philip. Energy band-gap engineering of graphene nanoribbons. Phys Rev Lett 2007;98:206805.
[17] Jiao Liying, Wang Xinran, Diankov Georgi, Wang Hailiang, Dai Hongjie. Facile synthesis of high-quality graphene nanoribbons. Nat Nano 5 2010;5:321–5.
[18] Jiao Liying, Zhang Li, Wang Xinran, Diankov Georgi, Dai Hongjie. Narrow graphene nanoribbons from carbon nanotubes. Nature 2009;458:877–80.
[19] Kittel C. Introduction to solid state physics. 3rd ed. New York: Wiley; 1967.
[20] Koskinen Pekka, Malola Sami, Häkkinen Hannu. Self-passivating edge reconstructions of graphene. Phys Rev Lett 2008;101:115502.
[21] Kosynkin Dmitry V, Higginbotham Amanda L, Sinitskii Alexander, Lomeda Jay R, Dimiev Ayrat, Katherine Price B, et al. Longitudinal unzipping of carbon nanotubes to form graphene nanoribbons. Nature 2009.
[22] Kuzmenko AB, van Heumen E, Carbone F, van der Marel D. Universal optical conductance of graphite. Phys Rev Lett 2008;100:117401.
[23] Larciprete Rosanna, Lacovig Paolo, Gardonio Sandra, Baraldi Alessandro, Lizzit Silvano. Atomic oxygen on graphite: chemical characterization and thermal reduction. J Phys Chem C 2012;116:9900–8.
[24] Lee Changgu, Wei Xiaoding, Kysar Jeffrey W, Hone James. Measurement of the elastic properties and intrinsic strength of monolayer graphene. Science 2008;321:385–8.
[25] Lee Hoonkyung. Preferential functionalization on zigzag graphene nanoribbons: first-principles calculations. J Phys: Condens Matter 2010;22:352205.
[26] Li Chuang, Zhao Anqi, Xia Wei, Liang Changhai, Muhler Martin. Quantitative studies on the oxygen and nitrogen functionalization of carbon nanotubes performed in the gas phase. J Phys Chem C 2012;116:20930–6.
[27] Li Xiaolin, Wang Xinran, Zhang Li, Lee Sangwon, Dai Hongjie. Chemically derived, ultrasmooth graphene nanoribbon semiconductors. Science 2008;319:1229–32.
[28] Hendrik Monkhorst J, James Pack D. Special points for Brillouin-zone integrations. Phys Rev B 1976;13:5188–92.
[29] Nakada Kyoko, Fujita Mitsutaka, Dresselhaus Gene, Dresselhaus Mildred S. Edge state in graphene ribbons: nanometer size effect and edge shape dependence. Phys Rev B 1996;54:17954–61.
[30] Nemes-Incze Péter, Magda Gábor, Kamarás Katalin, Biró László. Crystallographically selective nanopatterning of graphene on SiO_2. Nano Res 2010;3:110–6.
[31] Perdew John P, Burke Kieron, Ernzerhof Matthias. Generalized gradient approximation made simple. Phys Rev Lett 1996;77:3865–8.
[32] Reuter Karsten, Scheffler Matthias. Composition, structure, and stability of $RuO_2(110)$ as a function of oxygen pressure. Phys Rev B 2001;65:035406.
[33] Reuter Karsten, Scheffler Matthias. Composition and structure of the $RuO_2(110)$ surface in an O_2 and co environment: implications for the catalytic formation of CO_2. Phys Rev B 2003;68:045407.

[34] Salzmann Christoph G, Nicolosi Valeria, Green Malcolm LH. Edge-carboxylated graphene nanoflakes from nitric acid oxidised arc-discharge material. J Mater Chem 2010;20:314–9.
[35] Seitsonen Ari P, Marco Saitta A, Wassmann Tobias, Lazzeri Michele, Mauri Francesco. Structure and stability of graphene nanoribbons in oxygen, carbon dioxide, water, and ammonia. Phys Rev B 2010;82:115425.
[36] Silva-Tapia Alejandro B, García-Carmona Ximena, Radovic Ljubisa R. Similarities and differences in O_2 chemisorption on graphene nanoribbon vs. carbon nanotube. Carbon 2012;50:1152–62.
[37] Szabó Tamás, Berkesi Ottó, Dékány Imre. {DRIFT} study of deuterium-exchanged graphite oxide. Carbon 2005;43:3186–9.
[38] Tapaszto Levente, Dobrik Gergely, Lambin Philippe, Biro Laszlo P. Tailoring the atomic structure of graphene nanoribbons by scanning tunnelling microscope lithography. Nat Nano 2008;3:397–401.
[39] Valtiner Markus, Todorova Mira, Grundmeier Guido, Neugebauer Jörg. Temperature stabilized surface reconstructions at polar ZnO(0001). Phys Rev Lett 2009;103:065502.
[40] Vanderbilt David. Soft self-consistent pseudopotentials in a generalized eigenvalue formalism. Phys Rev B 1990;41:7892–5.
[41] Vanin M, Gath J, Thygesen KS, Jacobsen KW. First-principles calculations of graphene nanoribbons in gaseous environments: structural and electronic properties. Phys Rev B 2010;82:195411.
[42] Wang Hongtao, Feng Qiong, Cheng Yingchun, Yao Yingbang, Wang Qingxiao, Li Kun, et al. Atomic bonding between metal and graphene. J Phys Chem C 2013;117:4632–8.
[43] Wang Xinran, Ouyang Yijian, Li Xiaolin, Wang Hailiang, Guo Jing, Dai Hongjie. Room-temperature all-semiconducting sub-10-nm graphene nanoribbon field-effect transistors. Phys Rev Lett 2008;100:206803.
[44] Wang Xinran, Tabakman Scott M, Dai Hongjie. Atomic layer deposition of metal oxides on pristine and functionalized graphene. J Am Chem Soc 2008;130:8152–3.
[45] Xia Wei, Jin Chen, Kundu Shankhamala, Muhler Martin. A highly efficient gas-phase route for the oxygen functionalization of carbon nanotubes based on nitric acid vapor. Carbon 2009;47:919–22.